Received: 8 September 2023 | Revised: 18 October 2023 | Accepted: 19 October 2023 | Published online: 25 October 2023

RESEARCH ARTICLE

Journal of Optics and Photonics Research
2024, Vol. 1(2) 67–73
DOI: 10.47852/bonviewJOPR32021705

BON VIEW PUBLISHING

Characteristics Analysis of Different Photonic Crystal Fiber Lattice Structures

Lavanya Anbazhagan[1,*], P. Sudhanya[1] and R. Jansi[1]

[1]*Department of Electronics and Communication Engineering, SRM Institute of Science and Technology (Kattankulathur), India*

Abstract: This study presents a comprehensive analysis of various photonic crystal fiber (PCF) lattice structures using the Finite Element Method (FEM). PCFs have gained significant importance in various optical and communication applications due to their unique optical properties. Understanding the characteristics and optimal designs of different PCF lattice structures is crucial for their effective utilization. In this research, we explore eight distinct lattice designs, including circle, square, pentagon, hexagon, heptagon, octagon, decagon, and dodecagon. We investigate how variations in the air-filling fraction (AFF), a critical structural parameter, affect the performance of these PCF structures. The utilization of FEM allows for a detailed analysis of these lattice structures, offering insights into their behavior under different conditions. By varying the AFF, we gain valuable insights into the optimal design choices for specific applications. This research aims to provide a deeper understanding of the applicability of each PCF lattice structure. By scrutinizing their performance and characteristics, it becomes possible to distinguish which lattice structure is best suited for various optical and communication applications. The findings from this study offer significant contributions to the field of photonics, guiding researchers and engineers in selecting the most suitable PCF lattice structure for their specific applications. Understanding the structural parameters that influence PCF behavior is a key step toward optimizing the performance of optical and communication systems.

Keywords: characteristic analysis, different lattice structures, Finite Element Method, air-filling fraction

1. Introduction

Photonic crystal fiber (PCF) has indeed garnered significant attention in recent years due to its remarkable optical properties and versatile applications across various domains. The fascinating advantage of PCF is its design flexibility. Manipulating the structural parameters of PCFs allows for tailored optical properties like high birefringence, endless single-mode operation, large mode area, flat dispersion, and more, making PCF a versatile tool in photonics. In literature, different PCF lattice structures are investigated and attained desirable characteristics for various applications. The square lattice PCF with a very high negative dispersion of −2337.60 ps/nm-km and high nonlinear coefficient of 131.91 W^{-1} km^{-1} over 1340–1640 nm wavelength band is proposed [1]. A customized octagonal PCF has been engineered to exhibit a substantial negative dispersion ranging from −226 to −290 ps/nm km across the C- and L-bands, effectively serving as a broadband dispersion compensation solution [2]. The decagonal PCF consisting of unique cladding that has very high birefringence 1.02×10^{-2} with low confinement loss of 0.07771 dB/m at 1.55 μm is investigated [3]. Elliptical–spiral PCF that offers high birefringence of 0.05554, large nonlinearity of 3079 W^{-1} km^{-1}, and low chromatic dispersion of −95.45 ps/nm km in the wavelength range of 1000–1800 nm is explored [4]. In the communication wavelength range, a hybrid cladding photonic PCF demonstrated exceptional characteristics, including a remarkably high birefringence of approximately 10^{-2}, low confinement loss at 6.1×10^{-3} dB/km, a moderate negative dispersion of −274.5 ps/nm km, and a notably high nonlinearity of 76.41 W^{-1} km^{-1} [5]. Utilizing an eight-hexagonal-ring-structured PCF, remarkable optical properties were achieved, including a high nonlinearity of 116.76 W^{-1}·km^{-1} at 800 nm and a substantial negative dispersion of −650 ps/nm km at 1310 nm. This PCF enabled the generation of a broad supercontinuum spanning 600 nm in spectral range when exposed to a 50 fs pulse with a 2 kW pump power at an 800 nm wavelength [6].

Many different materials such as topaz, graphene, and fluorine are doped with silica to tailor the characteristics of the PCF. The octagonal PCF with fluorine doping in the core achieved a large effective mode area of 1110 μm^2 and an ultra-low confinement loss of 1.14×10^{-15} dB/m [7]. Chalcogenide glasses have garnered substantial interest in photonics and optical communications due to their notably high nonlinear coefficients, often exceeding silica's by two to three orders of magnitude. This unique attribute makes chalcogenide glasses exceptionally well-suited for a wide range of nonlinear applications, particularly when integrated with silica in the production of PCF, allowing for the creation of PCFs with significant refractive index contrast and exceptionally high nonlinearity [8]. A dual-cladding PCF featuring an elliptical As_2S_3

*Corresponding author: Lavanya Anbazhagan, Department of Electronics and Communication Engineering, SRM Institute of Science and Technology (Kattankulathur), India. Email: lavanyaa1@srmist.edu.in

core successfully attained remarkable optical characteristics. Notably, it achieved a high birefringence of 0.307, indicating a strong separation of polarized light propagation within the fiber, along with impressive nonlinear coefficients of 38,080 W^{-1} km^{-1}. These properties make it highly suitable for applications requiring controlled polarization and nonlinear optical effects [9]. A hybrid $AsSe_2$–As_2S_5 PCF with a solid elliptical core exhibited a very high birefringence of 0.091 and a large nonlinear coefficient of 147.8 [10]. A modified hexagonal tellurite PCF achieved a broadband ultra-flattened dispersion of 60 ps/nm km over 0.7 μm in the mid-infrared wavelength range and a very high nonlinear coefficient of 378.1 W^{-1} km^{-1}. With the designed PCF, a supercontinuum spectrum of 2900 nm is produced by injecting a pulse with a peak power of 5 Kw [11]. The design of a rotated porous core PCF has been tailored for the efficient propagation of terahertz (THz) waves. This PCF exhibits a dispersion of 1.06 ± 0.12 ps/THz/cm within the frequency range of 0.5–1.08 THz. Additionally, it demonstrates an impressively low material absorption loss of 0.066 cm^{-1} and minimal confinement loss, measured at 4.73 × 10^{-4} cm^{-1} at a frequency of 1 THz. These characteristics make it a promising candidate for various THz-wave-based applications where low dispersion, minimal absorption, and low loss are crucial [12].

The liquid infiltrated PCF is used for sensing applications. A modified hexagonal structure PCF has been ingeniously designed to accommodate liquid analytes infiltrated into the fiber core. This design showcases impressive sensitivity levels of 53.22%, 48.19%, and 55.56% for detecting ethanol, water, and benzene, respectively. These heightened sensitivities make it a valuable tool for applications that require precise and selective detection of these liquid analytes [13]. In a circular dual-core PCF, the infiltration of liquid analyte serves as a highly sensitive refractive index sensor. It exhibits an impressive maximum sensitivity of 22,071 nm/refractive index unit (RIU) when the refractive index of the liquid analyte is 1.41. Even at its minimum, it maintains a substantial sensitivity of 8929 nm/RIU when the refractive index is 1.33. This exceptional sensitivity range makes it a valuable tool for precise and responsive refractive index measurements in various applications [14]. TEC-PCF biosensors, designed for glucose detection with hemoglobin, utilize an asymmetric configuration for enhanced sensitivity. They offer a wide glucose concentration range (0–100 g/L) and perform best at 160 g/L hemoglobin, achieving sensitivities of 2.4 nm/(g/L) (X polarization) and 2.42 nm/(g/L) (Y polarization) at specific fiber lengths [15].

2. Material and Design

Figure 1 depicts the schematic layout of different PCF lattices such as the circle, square, pentagon, hexagon, heptagon, octagon, decagon, and dodecagon that are considered for this study. The ratio between the diameter of the air hole (d) and the pitch (∧) is called the air-filling fraction (AFF). The characteristic analysis is carried out for various AFF of 0.6, 0.7 and 0.8 for the wavelength range of 1.2–2 μm and the comparative study is also done.

3. Numerical Analysis

Silica is a common material used as the background or cladding material in many optical fibers, including PCFs. The refractive index of silica is wavelength-dependent, and this dependence is often described using the Sellmeier equation [16]:

Figure 1
Schematic layout of different PCF lattices. (a) Circle, (b) square, (c) pentagon, (d) hexagon, (e) heptagon, (f) octagon, (g) decagon and (h) dodecagon

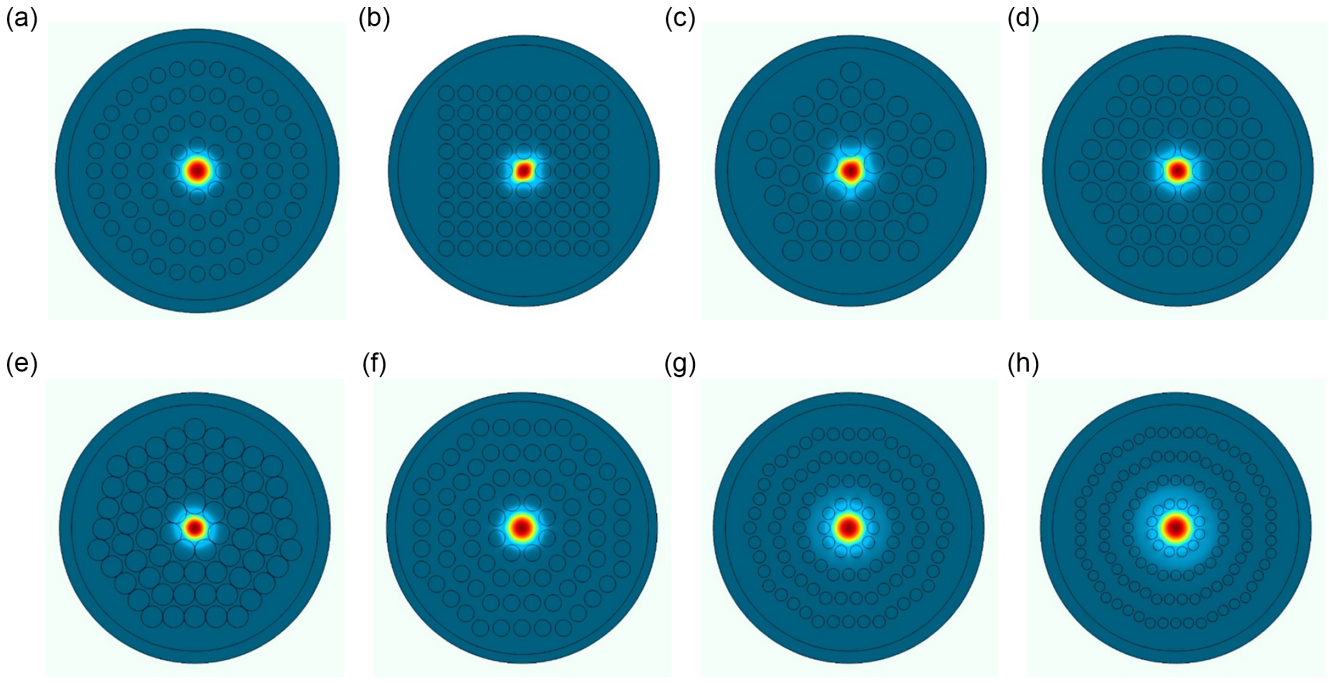

Table 1
Effective area and nonlinear coefficient of different PCF lattices at 1.55 μm

	Effective area (μm^2)			Nonlinear coefficient (W^{-1} km^{-1})		
Lattice type	AFF = 0.6	AFF = 0.7	AFF = 0.8	AFF = 0.6	AFF = 0.7	AFF = 0.8
Circle	3.65	3.23	2.84	33.32	37.63	42.75
Square	5.22	3.86	4.12	23.31	31.48	29.48
Pentagon	3.83	3.22	2.7	31.75	37.82	45.12
Hexagon	4.05	3.79	3.16	30.02	32.18	38.5
Heptagon	3.51	3.05	2.64	34.61	39.85	46.03
Octagon	8.57	7.84	7.1	14.18	15.5	17.12
Decagon	4.9	4.3	3.96	24.83	28.27	30.7
Dodecagon	5.45	4.61	3.77	22.3	26.4	32.25

$$n(\lambda) = \sqrt{1 + \frac{0.6961663\lambda^2}{\lambda^2 - 0.0684043^2} + \frac{0.4079426\lambda^2}{\lambda^2 - 0.1162414^2} + \frac{0.8974794\lambda^2}{\lambda^2 - 9.86161^2}} \quad (1)$$

Effective refractive index and the field distribution are determined by solving Maxwell's master wave equation [17]:

$$\nabla \times (\nabla \times E) - k_0^2 \in_r E = 0 \quad (2)$$

where k_0^2 is the eigenvalue and $\in_r$ is the relative permittivity.

Using the master wave equation, the important parameters that characterize the PCF are calculated as below [18]:

$$\text{Effective area } A_{eff} = \frac{\left[\iint |E(x,y)|^2 dx\, dy\right]^2}{\iint |E(x,y)|^4 dx\, dy} \quad (3)$$

$$\text{Nonlinear coefficient } \gamma = \frac{2\pi}{\lambda} \frac{n_2}{A_{eff}} \quad W^{-1}m^{-1} \quad (4)$$

$$\text{Confinement loss } \alpha = 8.686 \times \frac{2\pi}{\lambda} \times Im\left[n_{eff}\right] \times 10^3 \text{dB/Km} \quad (5)$$

$$\text{Numerical aperture } NA \approx \left(1 + \frac{\pi A_{eff}}{\lambda^2}\right)^{-\frac{1}{2}} \quad (6)$$

$$\text{Waveguide dispersion } D = -\frac{\lambda}{c} \frac{d^2\, Re\left[n_{eff}\right]}{d\lambda^2} \quad (7)$$

$$\text{Birefringence } B = |n_{eff}^x - n_{eff}^y| \quad (8)$$

where A_{eff} is the effective area expressed in μm^2; $E(x,y)$ is the electric field; λ is the operating wavelength; n_2 is the nonlinear refractive index ($n_2 = 3 \times 10^{-20}$ m^2 W^{-1} for silica); ^ is the pitch of the structure; n_{core} is the refractive index of the core, n_{cladding} is the refractive index of the cladding; $Im[n_{\text{eff}}]$ is the imaginary part of effective refractive index; $Re[n_{\text{eff}}]$ is the real part of effective refractive index, c is the velocity of light in free space; and n_{eff}^x and n_{eff}^y are the effective refractive indices of the two orthogonally polarized modes.

4. Results and Discussions

The utilization of COMSOL Multiphysics 5.2a, based on the Finite Element Method, for the analysis of various PCF lattice structures is a robust and effective approach. The AFF is varied for each PCF lattice structure, and the corresponding analysis is done as a function of wavelength. The characteristic analysis of each parameter is discussed below:

4.1. Effective area and nonlinear coefficient analysis

Effective area (A_{eff}) is a crucial factor for the PCF as it exerts influence on the light confinement in the core and also has a direct implication on the nonlinear coefficient (γ). A larger A_{eff} results in tighter light confinement, influencing key optical aspects like dispersion, nonlinear effects, and pulse propagation. Optimizing A_{eff} is crucial for tailoring the performance of PCFs in various optical applications. Since the effective area and the nonlinear coefficient are inversely correlated, the low effective area results in the large nonlinearity and vice versa. A thorough investigation has been conducted on different PCF lattice structures, with a focus on varying the AFF. The study includes an examination of the effective area and nonlinear coefficient for these various PCF lattice structures at different AFF values around the wavelength of 1.55 μm. The findings are presented in Table 1 of the research paper, to provide a comprehensive overview of the results and how the AFF impacts these key optical parameters.

The increase in AFF within PCF leads to a decrease in A_{eff}. This is due to the fact that as more of the cross-sectional area is occupied by air holes (higher AFF), there is a relatively smaller area left for the core. As a result, the effective area available for light confinement within the core diminishes. This reduction in effective area means that the light is less confined within the core and is more dispersed, affecting its guiding properties. Moreover, this rise in the AFF amplifies nonlinear behavior within the material, resulting in a higher nonlinear coefficient. The presence of air affects stress distribution and alters material properties, ultimately contributing to the heightened nonlinear effects. Thus, increasing AFF reduces effective area while enhancing the nonlinear coefficient. Notably, an AFF value of 0.8 stands out for its distinct characteristics, featuring a low effective area and a high nonlinear coefficient as observed from Table 1. Selecting an AFF value of 0.8 strikes a balance between achieving high nonlinearity while ensuring practicality in fabrication and handling.

The study has further investigated how the effective area and nonlinear coefficient of different PCF lattice structures vary with different AFF values across a range of wavelengths, providing insights into the complex interplay of these factors in optical design and applications. Figure 2 illustrates the extensive analysis of A_{eff} and γ for the different AFF of the heptagonal PCF, which acquired the high nonlinear coefficient.

The comprehensive exploration of A_{eff} and γ for the various PCF lattice structures at AFF of 0.8 is shown in Figure 3. The octagonal PCF has a low nonlinear coefficient compared to the other PCF lattice structures. The heptagonal PCF has the lowest effective area, which is followed by pentagonal, circular, and

Figure 2
Nonlinear coefficient and effective area of heptagonal PCF for different wavelength and AFF

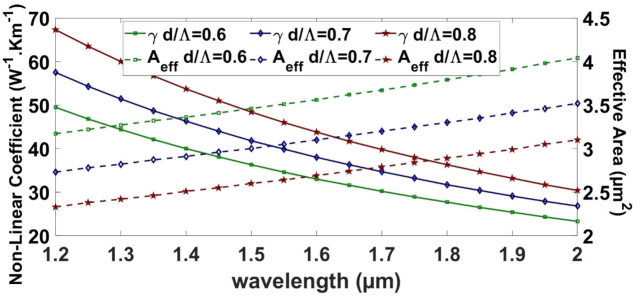

Figure 3
(a) Effective area and (b) nonlinear coefficient for different PCF lattices at AFF = 0.8

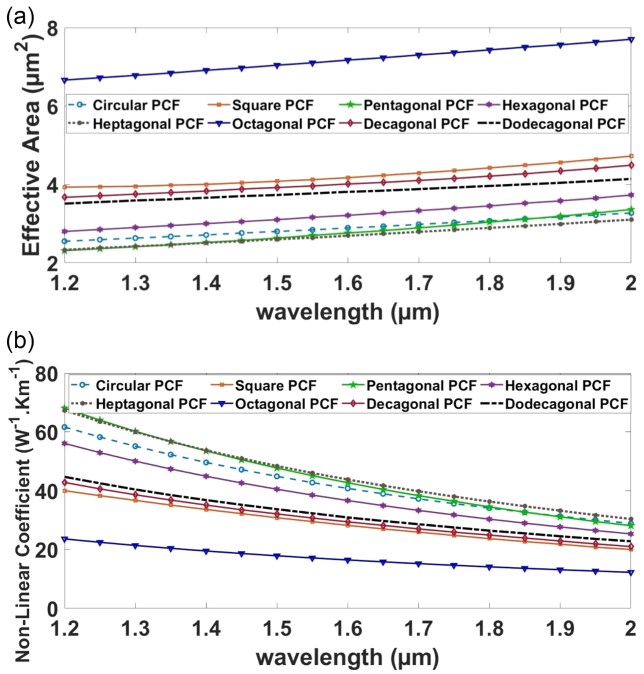

hexagonal PCFs, respectively. Thus, the heptagonal PCF is desirable for very high nonlinear applications.

4.2. Confinement loss analysis

Confinement loss, a critical metric in PCF analysis, characterizes the extent of light leakage within the PCF due to the evanescent field. The confinement loss across diverse PCF lattice structures has been meticulously evaluated, considering a range of AFF. The findings, summarized in Table 2, shed light on how different lattice structures and varying AFF values influence the extent of confinement loss in PCFs.

The study reveals a noteworthy trend in confinement loss concerning the AFF in PCF structures. As the AFF increases, the confinement loss diminishes significantly. Specifically, the octagonal PCF with an AFF of 0.8 stands out with the lowest confinement loss, measuring in the order of 10^{-7} at a wavelength

Table 2
Confinement loss characteristics of different PCF lattices at the wavelength of 1.55 μm

Confinement loss (dB/km)			
Lattice type	AFF = 0.6	AFF = 0.7	AFF = 0.8
Circle	4.35	1×10^{-2}	4.2×10^{-5}
Square	1.1×10^{2}	9.1×10^{-1}	4.9×10^{-3}
Pentagon	4.6×10^{1}	2.7×10^{-1}	1.6×10^{-3}
Hexagon	2.1×10^{-1}	3.4×10^{-2}	4.6×10^{-2}
Heptagon	0.5	1×10^{-3}	4.2×10^{-6}
Octagon	2.6×10^{-1}	8.5×10^{-4}	9.6×10^{-7}
Decagon	2.5×10^{4}	6.7×10^{2}	1.5×10^{1}
Dodecagon	1.4×10^{5}	6.9×10^{3}	4.3×10^{-1}

of 1.55 μm. In contrast, the heptagonal and circular PCF configurations exhibit relatively higher confinement losses, approximately in the order of 10^{-6} and 10^{-5}, respectively, at the same wavelength. These findings emphasize the importance of AFF in influencing the optical properties and performance of PCF structures.

In Figure 4, the relationship between the confinement loss of the octagonal PCF and various AFF values is illustrated. The data reveal a striking trend: with each increment of the AFF by a factor of 0.1, there is a substantial decrease in confinement loss, spanning two orders of magnitude. This trend underscores the critical role of the AFF in determining the PCF's optical characteristics. Notably, an AFF of 0.8 emerges as the optimal design choice, exhibiting the lowest confinement loss among the investigated AFF values.

Figure 4
The confinement loss of the octagonal PCF for the different AFF

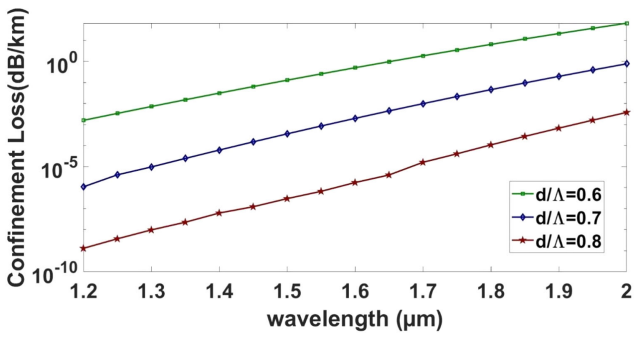

The extensive study on the confinement loss for different PCF lattice structures is deliberated in Figure 5. The decagonal and dodecagonal PCFs are found to have high confinement loss. Both the square and pentagonal PCFs have reasonable confinement loss in the order of 10^{-3}. The low confinement loss is reported in the octagonal PCF, which is followed by the heptagonal and circular PCF.

4.3. Numerical aperture analysis

The numerical aperture (NA) of a PCF serves as a crucial indicator of its capability to confine incident light rays effectively. Typically, a higher NA is preferred because it enhances the efficiency of light confinement. In the simulations conducted for various PCF lattice structures with different AFF values, it is clear

Figure 5
The confinement loss of different PCF lattice structures at AFF = 0.8

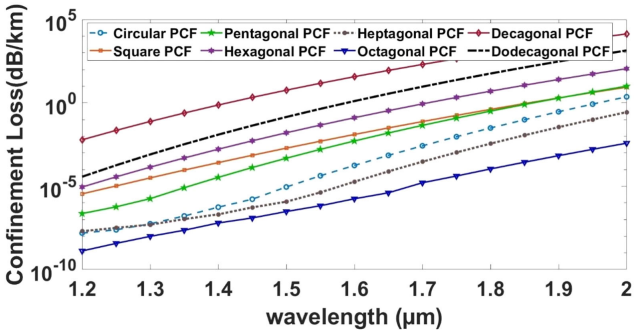

Figure 7
The numerical aperture of different PCF lattice structures at AFF = 0.8

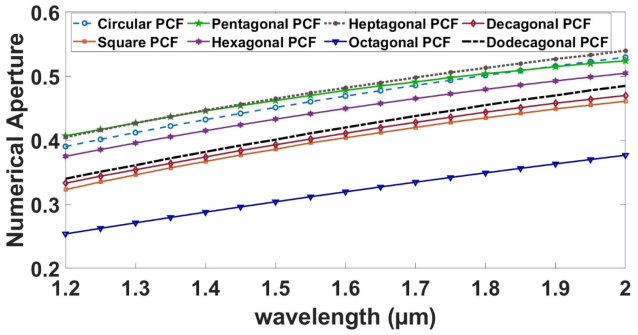

from Table 3 that the NA consistently increases with the increment in AFF. Remarkably, the pentagonal and heptagonal PCF lattice structures stand out with the highest NA, both measuring approximately 0.47 at the wavelength of 1.55 μm. These findings highlight the significance of NA in optimizing PCF design for enhanced light confinement and efficient optical performance.

Table 3
Numerical aperture of different PCF lattices at the wavelength of 1.55 μm

Lattice type	AFF = 0.6	AFF = 0.7	AFF = 0.8
Circle	0.416	0.437	0.460
Square	0.357	0.406	0.395
Pentagon	0.407	0.438	0.471
Hexagon	0.398	0.409	0.441
Heptagon	0.422	0.447	0.473
Octagon	0.286	0.298	0.311
Decagon	0.367	0.388	0.402
Dodecagon	0.351	0.377	0.416

Figure 6 elaborates the NA of the heptagonal PCF at different AFF. The value of NA increases linearly for all AFF in the wavelength range of 1.2–2 μm and also there is a surge in NA as the AFF increases.

The NA for the different PCF lattices at AFF=0.8 is investigated and plotted in Figure 7. The pentagonal and heptagonal PCF have similar NA for the wavelength less than 1.5 μm and after that, the pentagonal NA curve deviates and its slope decreases. The octagonal PCF has the minimum NA and the heptagonal PCF has the maximum NA.

Figure 6
The numerical aperture of the heptagonal PCF for the different AFF

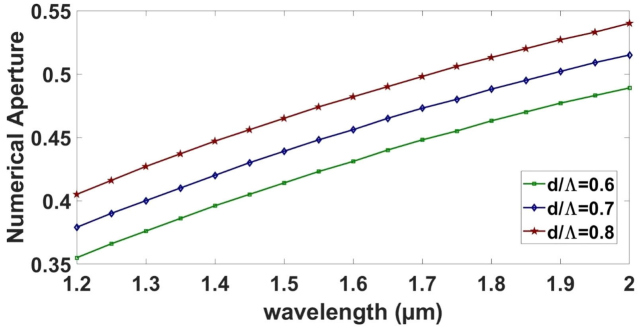

4.4. Dispersion analysis

When the light propagates inside the PCF, different frequency components progress with different group velocities, which results in dispersion. Even though the dispersion is an inevitable phenomenon, it can be engineered by varying the structural parameters of the PCF. Table 4 features the dispersion characteristics of the different PCF lattice structures at the wavelength of 1.55 μm.

Table 4
Dispersion of different PCF lattices at the wavelength of 1.55 μm

Dispersion(ps/nm km)			
Lattice type	AFF = 0.6	AFF = 0.7	AFF = 0.8
Circle	111.02	174.04	217
Square	72.56	105.42	128.98
Pentagon	100.86	126.34	145.26
Hexagon	75.33	97.44	141.59
Heptagon	128.90	175.37	217.51
Octagon	107.52	124.48	138.64
Decagon	−23.21	44.14	105.44
Dodecagon	−62.78	−0.3668	167.390

The minimum dispersion is necessary for the broadband communication applications. It is observed from Table 4 that the dispersion increases with the increase in the AFF. Since the dodecagonal PCF has the near-zero dispersion at the AFF of 0.7, it could indeed be a strong candidate for optical communication applications, particularly in scenarios where dispersion management is critical. The dispersion characteristics of the dodecagonal PCF for different AFF is shown in Figure 8.

Figure 9 exhibits the dispersion characteristics of the different PCF lattice structures at the AFF of 0.7. The circular PCF and the heptagonal PCF claim to have the flattened dispersion curve but have high dispersion value. The dodecagonal PCF has the minimum dispersion and also has sufficient ultra-flattened dispersion in the optical communication range.

Figure 8
Dispersion characteristics of the dodecagonal PCF at different AFF

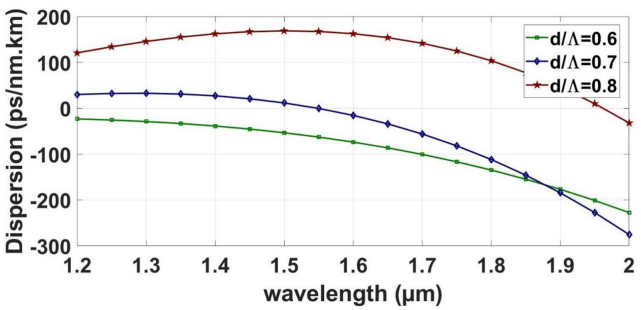

Figure 9
Dispersion characteristics of different PCF lattice structures at AFF = 0.8

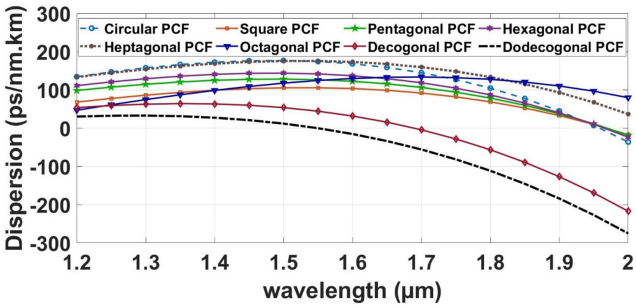

4.5. Birefringence analysis

The birefringence is the measure of the variation in the magnitude of the two perpendicularly polarized modes. The high birefringence behavior is desirable for polarization preserving application, as it results in the low beat length. Table 5 lists the birefringence of different PCF lattices at the wavelength of 1.55 μm.

Table 5
Birefringence of different PCF lattices at the wavelength of 1.55 μm

Lattice type	AFF = 0.6	AFF = 0.7	AFF = 0.8
Circle	7.9×10^{-7}	2.3×10^{-7}	1.29×10^{-7}
Square	3.8×10^{-8}	4.9×10^{-8}	1.9×10^{-7}
Pentagon	3.9×10^{-7}	1.2×10^{-6}	2×10^{-6}
Hexagon	6.1×10^{-8}	9.7×10^{-8}	2.5×10^{-7}
Heptagon	5.1×10^{-7}	6.4×10^{-7}	6.1×10^{-7}
Octagon	1.2×10^{-8}	2.1×10^{-8}	2.2×10^{-8}
Decagon	9.5×10^{-9}	3.8×10^{-8}	5.6×10^{-8}
Dodecagon	1×10^{-8}	3.1×10^{-8}	2.3×10^{-7}

Figure 10 depicts the detailed analysis of the birefringence of the pentagonal PCF at different AFF. The AFF of 0.6 and 0.7 has almost a flat birefringence curve in the wavelength range of 1.2–1.5 μm, whereas the AFF of 0.8 has a high birefringence curve with a gradually varying slope.

Figure 10
Birefringence of the pentagonal PCF at different AFF

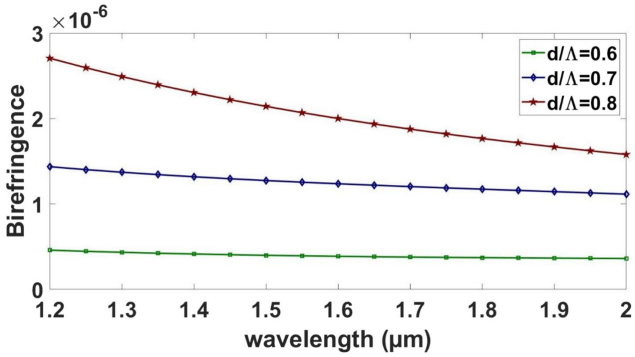

A comprehensive analysis of the birefringence characteristics has been carried out on the different PCF lattice structures, as shown in Figure 11. The pentagonal PCF displays a substantial birefringence, approximately on the order of 10^{-6}. In contrast, the circular, square, hexagonal, heptagonal, and dodecagonal PCFs exhibit birefringence in the range of 10^{-7}, equivalent to that of standard conventional fiber optics. Lastly, the octagonal and decagonal PCFs feature lower birefringence, measured at approximately 10^{-8}.

Figure 11
Birefringence of different PCF lattice structures at AFF = 0.8

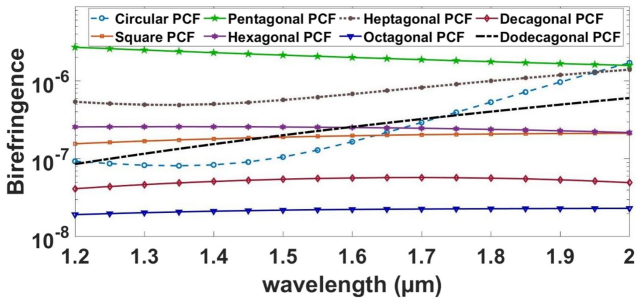

In addition to exploring diverse lattice structures in the design of PCFs, deliberate adjustments to the lattice, known as lattice errors, can also be introduced. An innovative hybrid hexagonal PCF design that integrates the golden ratio to achieve an elliptical core is emphasized by Lavanya and Geetha [19]. By utilizing the mathematical and proportional characteristics of the golden ratio and incorporating circular air holes, this unique PCF demonstrates exceptional optical properties, including negative dispersion, high birefringence, a substantial nonlinear coefficient, and a heightened NA. Integrating a dual-core structure into a PCF design has been shown to notably enhance the fiber's properties and functionalities. A novel approach using a silicon nanowire embedded dual-core pentagonal PCF for a polarization-independent wavelength splitter is presented [20]. Utilizing finite element analysis and coupled-mode theory, the PCF structure is optimized to achieve a coupling length ratio of 2. At different PCF lengths, impressive cross-talk suppression and bandwidths are achieved for both X and Y polarization modes, showcasing the potential of this PCF-based wavelength splitter for integrated optical systems. A diverse range of PCFs tailored to specific applications can be found throughout the existing literature. In

our investigation, we thoroughly analyzed the distinctive characteristics associated with various PCF lattice structures, assessing their suitability and potential across different optical applications.

5. Conclusion

In this comprehensive study, a detailed analysis was conducted on essential features of PCF, covering parameters such as effective area, nonlinear coefficient, confinement loss, NA, dispersion, and birefringence. Our investigation encompasses a range of PCF lattice structures, from circles to polygons like squares, pentagons, hexagons, heptagons, octagons, decagons, and dodecagons. Significantly, we have optimized the PCF design by systematically adjusting the AFF to attain the precise characteristics required for various optical applications. This versatile approach allows us to tailor PCF designs for specific needs, further advancing the field of photonics and optical communications.

Ethical Statement

This study does not contain any studies with human or animal subjects performed by any of the authors.

Conflicts of Interest

The authors declare that they have no conflicts of interest to this work.

Data Availability Statement

Data available on request from the corresponding author upon reasonable request.

References

[1] Islam, M. I., Khatun, M., & Ahmed, K. (2017). Ultra-high negative dispersion compensating square lattice based single mode photonic crystal fiber with high nonlinearity. *Optical Review*, *24*(2), 147–155. https://doi.org/10.1007/s10043-017-0308-0

[2] Kaijage, S. F., Namihira, Y., Hai, N. H., Begum, F., Razzak, S. M. A., Kinjo, T., . . . , & Zou, N. (2009). Broadband dispersion compensating octagonal photonic crystal fiber for optical communication applications. *Japanese Journal of Applied Physics*, *48*(5R), 052401. https://doi.org/10.1143/jjap.48.052401

[3] De, M., Gangwar, R. K., & Singh, V. K. (2017). Designing of highly birefringence, dispersion shifted decagonal photonic crystal fiber with low confinement loss. *Photonics and Nanostructures - Fundamentals and Applications*, *26*, 15–23. https://doi.org/10.1016/j.photonics.2017.06.002

[4] Gui, C., & Wang, J. (2012). Elliptical–spiral photonic crystal fibers with wideband high birefringence, large nonlinearity, and low dispersion. *IEEE Photonics Journal*, *4*(6), 2152–2158. https://doi.org/10.1109/jphot.2012.2226149

[5] Prabu, K., & Malavika, R. (2019). Highly birefringent photonic crystal fiber with hybrid cladding. *Optical Fiber Technology*, *47*, 21–26. https://doi.org/10.1016/j.yofte.2018.11.015

[6] Nair, A. A., Boopathi, C. S., Jayaraju, M., & Mani Rajan, M. S. (2019). Numerical investigation and analysis of flattened dispersion for supercontinuum generation at very low power using Hexagonal shaped Photonic crystal fiber (H-PCF). *Optik*, *179*, 718–725. https://doi.org/10.1016/j.ijleo.2018.11.021

[7] Kabir, S., & Razzak, S. M. A. (2018). An enhanced effective mode area fluorine doped octagonal photonic crystal fiber with extremely low loss. *Photonics and Nanostructures-Fundamentals and Applications*, *30*, 1–6. https://doi.org/10.1016/j.photonics.2018.02.002

[8] Markos, C., Yannopoulos, S. N., & Vlachos, K. (2012). Chalcogenide glass layers in silica photonic crystal fibers. *Optics Express*, *20*(14), 14814–14824. https://doi.org/10.1364/oe.20.014814

[9] Zhang, X., He, M., Chang, M., Chen, H., Chen, N., Qi, N., . . . , & Qin, X. (2018). Dual-cladding high-birefringence and high-nonlinearity photonic crystal fiber with As_2S_3 core. *Optics Communications*, *410*, 396–402. https://doi.org/10.1016/j.optcom.2017.10.026

[10] Yang, T., Ding, C., & Guo, Y. J. (2019). A highly birefringent and nonlinear $AsSe_2$ –As_2S_5 photonic crystal fiber with two zero-dispersion wavelengths. *IEEE Photonics Journal*, *11*(1), 7200307. https://doi.org/10.1109/jphot.2018.2886195

[11] Huang, T., Huang, P. M., Cheng, Z., Liao, J., Wu, X., & Pan, J. (2018). Design and analysis of a hexagonal tellurite photonic crystal fiber with broadband ultra-flattened dispersion in mid-IR. *Optik*, *167*, 144–149. https://doi.org/10.1016/j.ijleo.2018.04.016

[12] Islam, R., Hasanuzzaman, G. K. M., Habib, M. S., Rana, S., & Khan, M. A. G. (2015). Low-loss rotated porous core hexagonal single-mode fiber in THz regime. *Optical Fiber Technology*, *24*, 38–43. https://doi.org/10.1016/j.yofte.2015.04.006

[13] Islam, M. S., Paul, B. K., Ahmed, K., Asaduzzaman, S., Islam, M. I., Chowdhury, S., . . . , & Bahar, A. N. (2018). Liquid-infiltrated photonic crystal fiber for sensing purpose: Design and analysis. *Alexandria Engineering Journal*, *57*(3), 1459–1466. https://doi.org/10.1016/j.aej.2017.03.015

[14] Lou, J., Cheng, T., & Li, S. (2019). High sensitivity photonic crystal fiber sensor based on dual-core coupling with circular lattice. *Optical Fiber Technology*, *48*, 110–116. https://doi.org/10.1016/j.yofte.2018.12.023

[15] Vijayalakshmi, D., Manimegalai, C. T., Ayyanar, N., Vigneswaran, D., & Kalimuthu, K. (2021). Detection of blood glucose with hemoglobin content using compact photonic crystal fiber. *IEEE Transactions on NanoBioscience*, *20*(4), 436–443. https://doi.org/10.1109/TNB.2021.3097343

[16] Malitson, I. H. (1965). Interspecimen comparison of the refractive index of fused silica. *Journal of the Optical Society of America*, *55*(10), 1205–1209. https://doi.org/10.1364/josa.55.001205

[17] Knight, J. C., Birks, T. A., Atkin, D. M., & Russell, P. S. J. (1996). Pure silica single-mode fibre with hexagonal photonic crystal cladding. In *Optical Fiber Communication Conference, 2*, PD3.

[18] Agrawal, G. P. (2007). *Nonlinear fiber optics*. USA: Academic Press.

[19] Lavanya, A., & Geetha, G. (2020). A novel hybrid hexagonal photonic crystal fibre for optical fibre communication. *Optical Fiber Technology*, *59,* 102321. https://doi.org/10.1016/j.yofte.2020.102321

[20] Anbazhagan, L., & Ganesan, G. (2021). Polarization-independent wavelength splitter based on silicon nanowire embedded dual-core pentagonal lattice photonic crystal fiber for optical communication systems. *Optical Engineering*, *60*(4), 047103. https://doi.org/10.1117/1.oe.60.4.047103

How to Cite: Anbazhagan, L., Sudhanya, P., & Jansi, R. (2024). Characteristics Analysis of Different Photonic Crystal Fiber Lattice Structures. *Journal of Optics and Photonics Research*, *1*(2), 67–73. https://doi.org/10.47852/bonviewJOPR32021705